




Morphological instability and mobility of the color front during the electrocoloration of perovskite oxide thin films

Heung-Sik Park , Ji Soo Lim, Jeonghun Suh , and Chan-Ho Yang *

Department of Physics, Korea Advanced Institute of Science and Technology, Yuseong-gu, Daejeon 34141, Republic of Korea and Center for Lattice Defectronics, Korea Advanced Institute of Science and Technology, Yuseong-gu, Daejeon 34141, Republic of Korea



(Received 1 September 2023; accepted 20 November 2023; published 15 December 2023)

Visualization of dynamic processes during ionic migration in oxides can provide us opportunities for direct observation of various ionic phenomena and for understanding mechanisms of various applications that work based on ionic migration in solids. Electrocoloration is a readily accessible means of the direct observation of dynamic processes governed by oxygen ion migration. Here, we investigate the dynamic behavior of color fronts in the lateral devices of Ca-doped BiFeO₃ thin films grown on SrTiO₃ (100) substrates by recording the electrocoloration process with an optical microscope while simultaneously measuring the channel current. Voltage-dependent morphological instabilities, such as kinetic roughening of color fronts, are analyzed. We found that a significant amount of oxidation preceded the propagation of color fronts during electrocoloration and hence oxygen ionic mobility measured from the electrocoloration methods is the property of the intermediate phase, more oxidized than the pristine phase. This work provides intriguing insights into the dynamic behaviors of oxygen ions in oxides and the ionic mobility measurements with electrocoloration methods.

DOI: [10.1103/PhysRevMaterials.7.123401](https://doi.org/10.1103/PhysRevMaterials.7.123401)

I. INTRODUCTION

Various next-generation applications, such as solid oxide fuel cells [1–3], resistive random access memories [4–6], electrochromic windows [7,8], and solid-state batteries [9,10], work on the basis of ionic migration in solids. Thus, direct visualization of ionic migration in solids can provide us with fruitful information for observing various ionic phenomena and understanding the devices' mechanisms. Many methodologies, such as *in situ* x-ray diffraction [11], conductive atomic force microscopy [12], transmission electron microscopy [13,14], atom probe tomography [15], and time-of-flight secondary-ion-mass-spectroscopy [16] are utilized as a tool for studying the kinetics of mobile ions in solids. However, it remains challenging to observe the dynamic behavior both in real time and space because of several reasons such as poor spatial resolution, a light atomic mass of mobile ions, or the destructive nature of measurement tools. Given that the direct visualization of ionic motions has been challenging, the dynamic processes occurring with the spatial redistribution of oxygen ions are not fully understood. For example, there were many contentions about the growth direction of conducting filaments in resistive random access memories [17].

Electrocoloration can be a complementary tool capable of directly visualizing the dynamic behaviors of oxygen ions in oxides. Local color changes induced by oxygen ionic migration can be visualized by optical microscopy, providing an easily accessible platform for modeling oxygen ions by varying external parameters such as the applied voltage and

by measuring the channel current simultaneously. Electrocoloration has been a traditional method to study the resistance degradation mechanisms of perovskite oxides, such as BaTiO₃ [18] and SrTiO₃ [19–22]. Conventional models for describing electrocoloration processes consider systems composed of a binary phase and corresponding moving interface [18,19]. The binary phase consists of an infinitely conducting oxidized phase and an insulating phase with constant conductivity [Fig. 1(a)]. Since those two phases are connected in series, the entire voltage is considered to be applied across the insulating region, with Ohm's law:

$$\frac{V}{I} = \frac{L-x}{A\sigma_{\text{tot}}}, \quad (1)$$

where V is the applied voltage, I is the total current, L is the length of the channel, x is the position of the color front, A is the cross-sectional area of the channel, and σ_{tot} is the total conductivity of the insulating phase. On the other hand, color front mobility is expressed as

$$\mu_b = \frac{v_b}{E} = \frac{v_b(L-x)}{V} = \frac{v_b A}{I} \sigma_{\text{tot}}, \quad (2)$$

where v_b is the velocity of color front, and E is the electric field across the insulating phase. Generally, the rate-determining step for color front propagation is considered as the oxygen ionic migration [18,19]. Therefore, the mobility of the color front can be interpreted as the mobility of oxygen ions. Determination of the oxygen ionic mobility in oxides has been essential for various purposes, such as for estimations of the degradation rates of oxide capacitors [18] and for discovering candidate materials for solid oxide fuel cells with high oxygen ionic diffusivities at lower temperatures [23]. Recently, oxygen ionic mobilities determined from

*Corresponding author: chyang@kaist.ac.kr

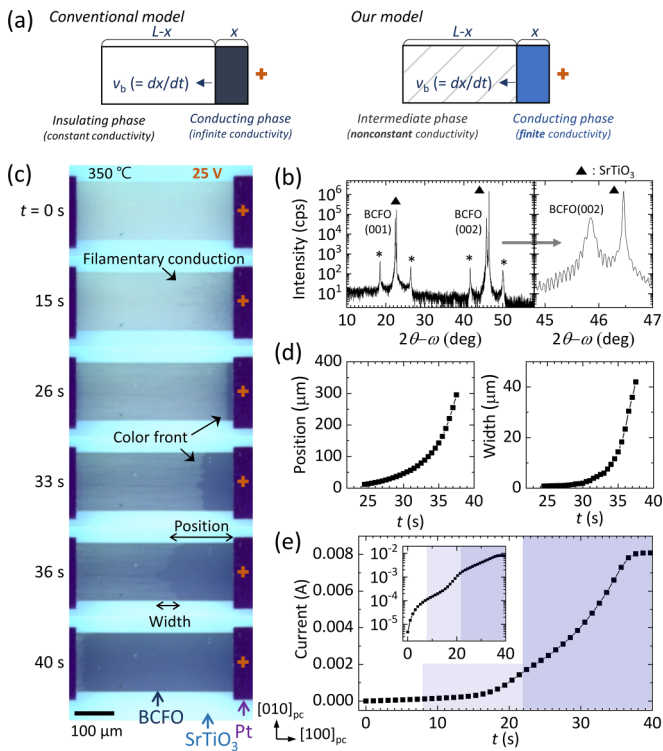


FIG. 1. Basic characterization of the sample and the electrocoloration experiment. (a) Schematic representation for the models describing electrocoloration processes. (b) X-ray diffraction $2\theta-\omega$ scan of a BCFO/SrTiO₃ thin film. Peaks noted with asterisk (*) indicate oxygen vacancy orderings. (c) Optical microscopy images during electrocoloration where 25 V was applied at 350° C (multimedia available online). (d) Evolution of position and width of the color front. (e) Current during electrocoloration. Pale-shadowed regime corresponds to the propagation of the intermediate phase composed of the dark filaments and deep-shadowed regime corresponds to the propagation of the color front.

electrocoloration experiments in Ca-doped BiFeO₃ (Bi_{1-x}Ca_xFeO_{3-δ}; BCFO) were found to be consistent with those measured by electrochemical impedance spectroscopy [23,24].

However, the conventional model needs to be revised for a better understanding of the electrocoloration process and the ionic mobility measured from it. Fitting curves established from the model showed non-negligible deviations from the real data [19,23]. Yoo *et al.* reported that the color front mobilities of doped BaTiO₃ single crystals had little dependency on the impurity types and contents [18]. The mechanism of the impurity independency has not been explained yet. These reports in the literature motivate us to establish the more appropriate model for describing the electrocoloration process.

Meanwhile, another interesting outcome related to the dynamic behaviors during electrocoloration was noted: the width, or roughness, of the color fronts. Roughening of growing surfaces, also known as kinetic roughening, has been widely studied in various types of physical systems, such as ferroelectric domain walls [25] and epitaxial growth [26] and fluid invasion processes [27–29]. In electrocoloration, the stability criterion for kinetic roughening was described

by Schmalzried [30]. Several studies experimentally reported unstable morphologies of the color front in BaTiO₃ [18], yttria-stabilized zirconia [31], and BCFO [32]. However, the evolution of the width with morphological instability was not a main concern of earlier authors.

BCFO is a useful model material for investigating the dynamic behaviors of oxygen ions in oxides. Aliovalent substitution of Ca²⁺ for Bi³⁺ produces a large number of oxygen vacancies. In pristine BCFO, the number of oxygen vacancies is proportional to the Ca content, i.e., $\delta = x/2$ [33]. The spontaneously produced oxygen vacancies facilitate ionic diffusion in this material. Low activation energy (~ 0.43 eV) for oxygen ionic diffusivity was reported for BCFO at $x = 0.45$ [23]. Under electrical bias at an elevated temperature, oxygen ions were redistributed, and an oxidized phase, in which nearly all oxygen vacancies were removed according to x-ray photoelectron spectroscopy [34], could be generated. In addition, BCFO has strong electrochromism, which makes it a good material for electrocoloration studies [35].

Here, we quantitatively analyze the dynamics of the color front during the electrocoloration of BCFO thin films at $x = 0.3$ grown on SrTiO₃ (100) substrates. In the first part, the kinetic roughening and morphological instability of the color fronts are reported. In the second part, the mobility of the color front is carefully studied with a revised model proposed for electrocoloration dynamics. Discussion about the question of whether the measured ionic mobility are about the pristine phase or about the intermediate phase, which is more oxidized than the pristine phase, is given. The oxygen ionic mobility of the BCFO thin film determined with our model is compared with outcomes in the literature.

BCFO thin films were grown on SrTiO₃ (100) substrates by pulsed laser deposition (see Ref. [32] for detailed information about sample synthesis). Figure 1(b) presents the x-ray diffraction $2\theta-\omega$ scan of the BCFO thin film, revealing its epitaxial growth. The satellite peaks marked with asterisks in Fig. 1(b) originate from the modulation of the crystal structure by every five pseudocubic unit cells along the c axis due to oxygen vacancy ordering [36]. The film thickness was determined to be 100 nm from the periodicity of a fringe structure near the Bragg peak. Lateral devices were fabricated for electrocoloration experiments. In this case, 400-μm-long BCFO channels were fabricated by Ar ion milling. Subsequently, a 10-nm-thick transparent LaAlO₃ capping layer was deposited on top of the device. Given that LaAlO₃ has large formation energy for oxygen vacancies, it can act as a capping layer to prevent oxygen exchange between the atmosphere and the thin film [37,38]. Pt electrodes were deposited onto both sides of the channels after slight Ar ion milling to remove the LaAlO₃ capping layer at the region intended for Pt deposition.

II. OBSERVATION OF ELECTROCOLORATION WITH CURRENT MONITORING

Figure 1(c) presents optical microscopy images taken during electrocoloration at an elevated temperature, in this case 350° C (for a video, see the Supplemental Material [39]). Note that the analyzer was positioned and aligned to be perpendicular to the polarizer of the optical microscope because doing so leads to better contrast for the detection of color fronts by

darkening the conducting phase. Positive voltage was applied to the electrode on the right side, i.e., the anode. The color of the pristine BCFO sample, i.e., $\delta = x/2 = 0.15$, was bright [Fig. 1(c)]. After 8 s of applied voltage, an intermediate phase nucleated from the anode and propagated toward the cathode ($t = 15$ s). The intermediate phase was composed of dark filaments growing along the crystal axes [40]. From $t = 22$ s, a color front appeared from the anode and propagated toward the cathode ($t = 26, 33,$ and 36 s). Furthermore, the color front exhibited an increasingly undulating shape over time. After a sufficiently long time, almost the entire channels except the narrow region near the ground electrode became dark and the color front nearly reached the cathode. All oxygen vacancies were removed in the dark phase, i.e., $\delta = 0$ ($t = 40$ s) [34]. The narrow region near the ground electrode, persistent even after the electrocoloration process was finished and a current was saturated, is an oxygen-vacancy-rich phase that acts as a sink for the removed oxygen vacancies near the positive electrode. The position and width of the color front were quantitatively tracked [Fig. 1(d)]. The position of the color front was defined as the average of the normal distances from the anode, and the width was defined as the standard deviation of the normal distances from the average position. Both the position and width grew over time while accelerating, and the width evolution demonstrated more dramatic acceleration. The electrocoloration process was accompanied by resistance degradation of more than three orders of magnitude [Fig. 1(e)]. At the initial stage, several μA of current was flowing. Until 8 s, the current increased more than an order of magnitude even though there was little change of apparent color in the channel. While an intermediate phase composed of the dark filamentary conduction paths extended, the current increased with an additional one order of magnitude to several mA. Finally, during the propagation of the color front, the current increased from 2 to 8 mA. These observations indicated that a significant amount of oxidation had already occurred in the channel, even before a color front appeared near the positive electrode.

III. MORPHOLOGICAL INSTABILITY OF THE COLOR FRONT

The propagation and roughening of the color front could be understood by considering the model described in earlier work, for which with schematic images are shown here [Fig. 2(a)] [30]. In Fig. 2(a), the white dashed region indicates an intermediate phase, and the blue region indicates a completely oxidized conducting phase. Under electrical bias, oxygen ions flowing through the intermediate phase accumulate at the color front and therefore extend the conducting phase, leading to the propagation of the color front. If the oxygen ionic conductivity of the intermediate phase is weaker than the electronic conductivity of the oxidized conducting phase, the oxygen ionic current through the intermediate phase becomes the rate-determining step in the propagation of the color fronts. In the presence of a small fluctuation in the roughness of the color front, oxygen ions tended to accumulate more at protruding regions, where stronger electric fields were concentrated. This gives rise to amplification of the roughness, or instability [30,31].

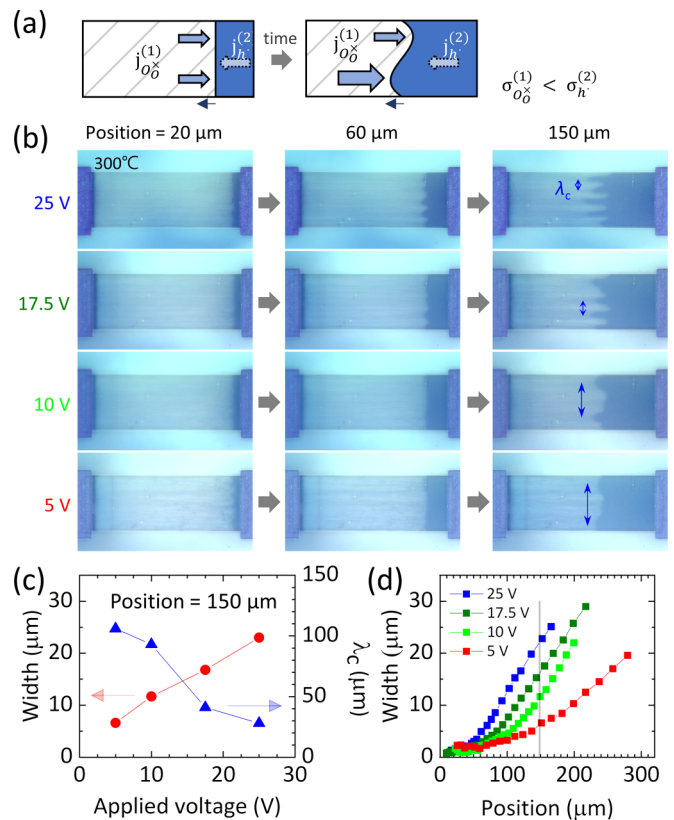


FIG. 2. Morphological instability of the color fronts. (a) Schematic representation of kinetic roughening of color fronts. (b) Images captured when the position of the color fronts reached 20, 60, and 150 μm , under various applied voltages at 300°C. (c) Width and most-unstable wavelength, λ_c , as a function of applied voltages. (d) Width as a function of position with different applied voltages.

The morphological instability exhibited voltage dependency. Figure 2(b) presents images during electrocoloration with different applied voltages captured when the position reached 20, 60, and 150 μm . At the initial stages, all color fronts showed flat surfaces. As time elapsed, color fronts with higher voltages showed greater roughness levels. When the position reached 150 μm , all images exhibited rough color fronts. Furthermore, the color fronts with higher voltages had fingerlike structures. Here, we introduced an additional parameter, called the most unstable wavelength, λ_c , defined as the shortest distance between the protruding fingerlike structures as indicated in Fig. 2(b). The width increased and λ_c decreased as the applied voltage was increased [Fig. 2(c)], both indicating greater instability under stronger applied voltages. Except for very early stages, i.e., when the widths were narrower than 3 μm , the widths were generally wider under stronger applied voltages as shown in the position-dependent plot of width in Fig. 2(d). The cause for the wider width at lower voltages in the early stages may be related to the filamentary conduction pathways preceding the propagation of the color front. The images taken at 5 V shown in Fig. 2(b) present more inhomogeneous textures in the intermediate phase due to the greater inhomogeneity arising during the formation of filamentary conduction pathways at lower voltages. This could induce a certain amount of unstable propagation

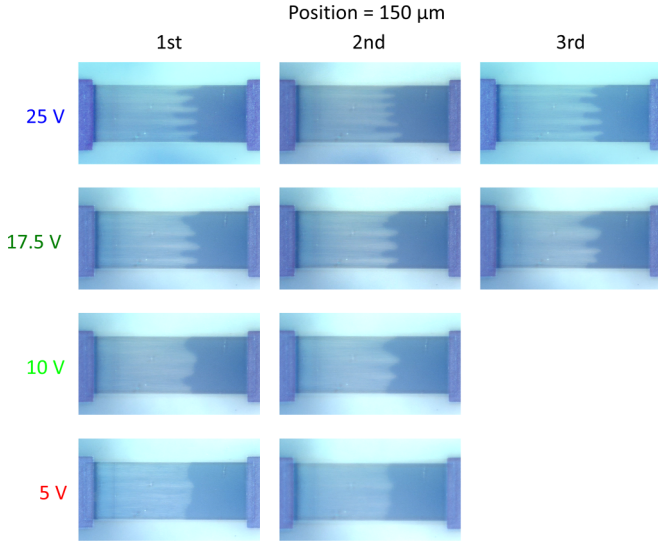


FIG. 3. Morphological retention of the color fronts. Images captured when the position reached $150 \mu\text{m}$ for repeated trials of electrocoloration.

of the color front at the beginning of the electrocoloration process with weakly applied voltages. Time-dependent plots of position and width are also presented in the Supplemental Material [39].

These voltage dependencies of the morphological instability are not explicitly contained in the model shown in Fig. 2(a), although there was another experimental case that reported qualitatively determined voltage dependencies of the widths of color fronts [31]. Here, we note that our tendencies can be interpreted, at least phenomenologically, using the concept of fluid dynamics. When a fluid with lower viscosity displaces a fluid with higher viscosity, fingerlike boundaries can form, as shown in the electrocoloration experiments. In this system, λ_c was inversely proportional to the square root of the fluid-injection speed [27,29,42]. In addition, injection-speed-dependent morphological transformation from stable to unstable fronts has been reported in another system involving fluid invasion [28].

In some physical systems, such as ferroelectric domain walls, kinetic roughening is strongly affected by pre-existing defects distributed within a sample. In other cases, such as epitaxial growth, kinetic roughening should be a purely stochastic behavior under a given model. Our system is likely to be the former case. Figure 3 presents images from repeated electrocoloration processes under given applied voltages captured when the position reached $150 \mu\text{m}$. The overall shapes of the color front with the same voltages very closely resemble each other, suggesting that the color front propagation was hardly a purely stochastic process but was instead affected by the internal defect distribution, which was not randomized within several trials of electrocoloration. Questions about the exact type of defect distribution governing the shape of color fronts are beyond the scope of this work. Although the general shapes were similar, they were not completely identical, meaning that the original shapes of the color fronts would become increasingly distorted as the number of repeated electrocoloration steps increased, and at some point, beyond the

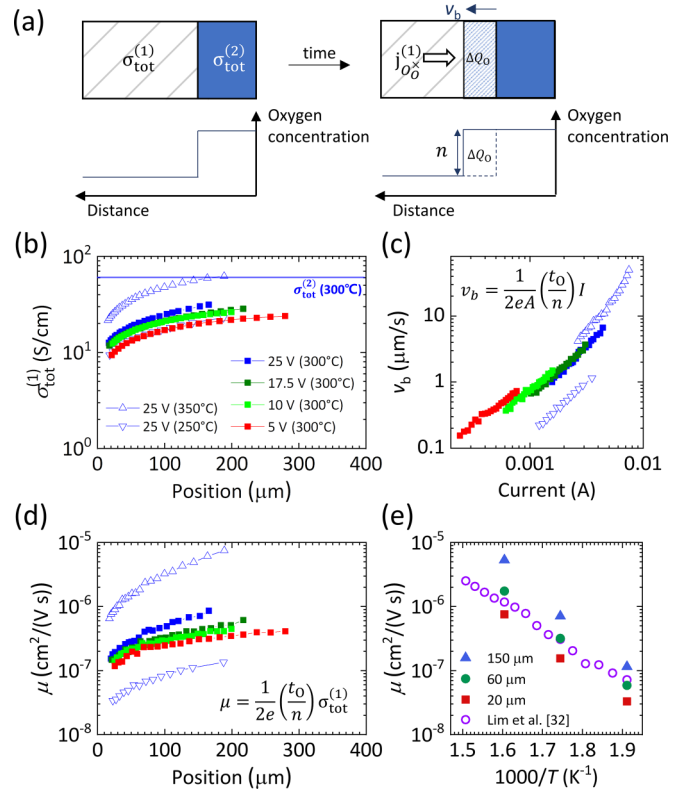


FIG. 4. Model for color front propagation and determination of the oxygen ionic mobility. (a) Schematic picture of the model for the color front propagation. (b) Conductivities of the intermediate phase as a function of position with different applied voltages and temperatures. (c) Color front velocities as a function of current. (d) Oxygen ionic mobilities as a function of position. (e) Arrhenius plot of the oxygen ionic mobilities under 25 V, compared with Ref. [32].

retention ability, the information pertaining to the original shape would be lost.

IV. MOBILITY OF THE COLOR FRONT

In contrast to the fact that instances of morphological instability in electrocoloration have not been investigated thus far, color front mobility has been examined in a range of previous studies. One of the main outcomes of a color front analysis is the determination of the oxygen ionic mobility from the conventional model with Eqs. (1) and (2). In this study, we propose a revised model that assumes nonconstant conductivity of the intermediate phase and finite conductivity of the conducting phase [Fig. 4(a)]. At arbitrary times, Ohm's law leads to the following relationship:

$$\frac{V}{I(t)} = \frac{L - x(t)}{A\sigma_{\text{tot}}^{(1)}(x, V)} + \frac{x(t)}{A\sigma_{\text{tot}}^{(2)}}, \quad (3)$$

where $\sigma_{\text{tot}}^{(1)}$ is the total conductivity of the intermediate phase, and $\sigma_{\text{tot}}^{(2)}$ is the total conductivity of the conducting phase. $\sigma_{\text{tot}}^{(2)}$ was calculated and found to be 60 S/cm at 300°C from the saturation current at the end of the electrocoloration process at 25 V when mostly the entire BCFO channel became oxidized. Figure 4(b) shows that $\sigma_{\text{tot}}^{(1)}$ increases as the color front propagates. Furthermore, it is higher when higher voltage is applied.

$\sigma_{\text{tot}}^{(1)}$ and $\sigma_{\text{tot}}^{(2)}$ were even on the same order of magnitude, indicating that the intermediate phase had already undergone a significant amount of oxidation from the beginning of color front propagation, as already observed in Fig. 1(e). Although the current flowing through the intermediate phase came from the corresponding mixed ionic-electronic conduction, the propagation of a color front provided us with information about the pure oxygen ionic current. The velocity of the color front and the mixed conductivity of the intermediate phase can be related to each other, as follows:

$$\frac{dQ_O}{dt} = t_O(x, V)I(t) = 2eA \cdot v_b(t) \cdot n(x, V), \quad (4)$$

where Q_O is the charge of oxygen ions accumulated near the color front, t_O is the transference number for oxygen ionic current, v_b is the velocity of the color front, e is the electronic charge, and n is the oxygen vacancy concentration. Therefore, the velocity of the color front can be expressed as a function of the total current, as follows:

$$v_b(x, V, t) = \frac{1}{2eA} \left(\frac{t_O(x, V)}{n(x, V)} \right) I(t). \quad (5)$$

In this way, an unknown parameter t_O/n can be determined from the velocity versus total current results [Fig. 4(c)]. Finally, the oxygen ion mobility can be written as follows:

$$\begin{aligned} \mu(x, V) &= \frac{v_O}{E^{(1)}(x, V)} = \frac{\frac{1}{2eA} \frac{t_O}{n}}{E^{(1)}(x, V)} \\ &= \frac{1}{2e} \left(\frac{t_O(x, V)}{n(x, V)} \right) \sigma_{\text{tot}}^{(1)}(x, V), \end{aligned} \quad (6)$$

where μ is the mobility of the oxygen ions, v_O is the drift velocity of the oxygen ions in the intermediate phase, and $E^{(1)}$ is the electric field in the intermediate phase [Fig. 4(d)]. Even at the same temperature, the mobility depended on the position of the color front and the applied voltage. As mentioned earlier, this occurred because the intermediate phase oxidized over time. The oxidation affected both $\sigma_{\text{tot}}^{(1)}$ and t_O/n , leading to an increase in the mobility during electrocoloration. These observations provided us with a hint about the origin of the impurity-independent mechanism of color fronts reported by Yoo *et al.* [18]. The mobility levels determined from the electrocoloration experiments were related to the intermediate phase, where a significant amount of oxidation had already occurred from the pristine phase. Regardless of the types of and amounts of impurity doped into the pristine phase, the initial differences became relatively negligible after the significant oxidation that occurred during the formation of the intermediate phase. Figure 4(e) presents the mobility outcomes as determined from three different positions (20, 60, and 150 μm) when 25 V was applied at 250, 300, and 350° C. These results were compared to others in the literature [32], where the mobility values of BCFO with $x = 0.3$ grown on SrTiO₃ (100) were determined using the conventional model of constant mobility independent of the position.

The color front movements were nearly at constant velocities under constant currents [Fig. 5(a)]. The average velocities calculated from the slope of the linear fitting curve are shown in Fig. 5(b). The average velocities were linearly proportional

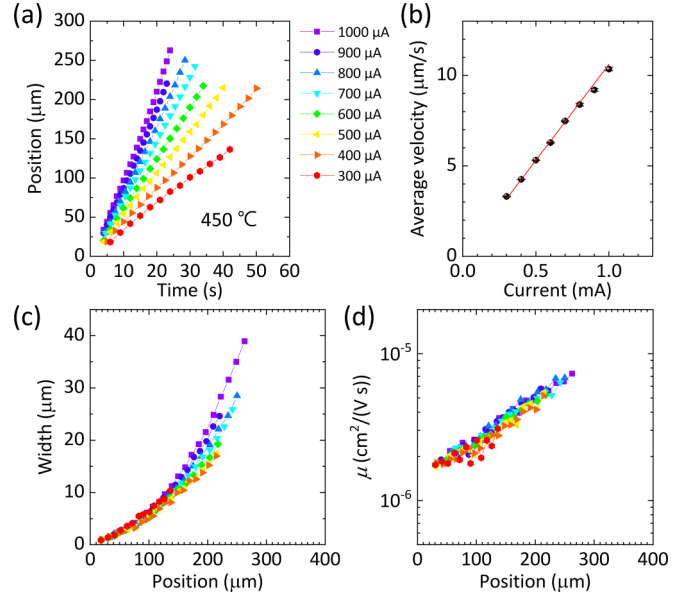


FIG. 5. Color front dynamics under constant currents. (a) Evolution of position under constant currents at 450° C. (b) Average velocity proportional to applied currents. (c) Evolution of width under constant currents. (d) Oxygen ionic mobilities of the intermediate phase as a function of position.

to the current. Kinetic roughening was also observed under a constant current, and color fronts had larger widths when higher currents were flowing [Fig. 5(c)]. The mobility levels were determined using methods similar to those used in the constant voltage experiments [43]. In contrast to the experiments with constant voltages, the mobility versus position relationships overlapped along a single curve.

V. CONCLUSION

In summary, we quantitatively studied the dynamics of color fronts during electrocoloration in BCFO thin films, focusing on morphological instability and the mobility of the color fronts. In the first part, kinetic roughening was reported with quantitative measurements of the position and width of the color fronts. Instances of voltage-dependent morphological instability as expressed by the widths and the most unstable wavelength, λ_c , were observed. The general shapes of the color fronts were retained within several trials of electrocoloration when the same voltage magnitudes were applied. In the second part, we measured the color front mobilities and found that the pristine insulating phase kept changing to the more conducting phase during color front propagation and its conductivities were comparable to the conductivity of the conducting phase, by establishing the revised model which modified basic assumptions for the conventional model. A significant amount of oxidation was already occurring even before the appearance of the color front and this observation led us to conclude that the color front mobilities reflected the ionic mobilities of the intermediate phase, not of the pristine phase. Last, the color fronts moved with constant velocities under constant currents. The mobility versus position relationship was found to be on a single curve

with various currents. Our studies of the dynamics of electrocoloration processes will provide interesting insights into the dynamics of oxygen ions in oxides and the measurements of ionic mobilities.

ACKNOWLEDGMENTS

This work was supported by a National Research Foundation (NRF) grant funded by the Korean government via the

Creative Research Initiative Center for Lattice Defectronics (Grant No. 2017R1A3B1023686).

C.-H.Y. supervised the project. H.-S.P., J.S.L., and J.S. prepared the samples and fabricated devices for the experiments. H.-S.P. performed electrocoloration experiments. H.-S.P. analyzed experimental data. H.-S.P. and C.-H.Y. wrote the manuscript.

The authors have no conflicts to disclose.

-
- [1] V. V. Kharton, F. M. B. Marques and A. Atkinson, Transport properties of solid oxide electrolyte ceramics: A brief review, *Solid State Ion.* **174**, 135 (2004).
- [2] J. Zhang, S. Ricote, P. V. Hendriksen and Y. Chen, Advanced materials for thin-film solid oxide fuel cells: Recent progress and challenges in boosting the device performance at low temperatures, *Adv. Funct. Mater.* **32**, 2111205 (2022).
- [3] Z. Gao, L. V. Mogni, E. C. Miller, J. G. Railsback and S. A. Barnett, A perspective on low-temperature solid oxide fuel cells, *Energy Environ. Sci.* **9**, 1602 (2016).
- [4] J. S. Lee, S. Lee, and T. W. Noh, Resistive switching phenomena: A review of statistical physics approaches, *Appl. Phys. Rev.* **2**, 031303 (2015).
- [5] R. Waser and M. Aono, Nanoionics-based resistive switching memories, *Nat. Mater.* **6**, 833 (2007).
- [6] K. M. Kim, D. S. Jeong, and C. S. Hwang, Nanofilamentary resistive switching in binary oxide system; a review on the present status and outlook, *Nanotechnology* **22**, 254002 (2011).
- [7] S. K. Deb, Opportunities and challenges in science and technology of WO₃ for electrochromic and related applications, *Sol. Energy Mater. Sol. Cells* **92**, 245 (2008).
- [8] C. G. Granqvist, A. Azensb, P. Heszlerc, L. B. Kishd, and L. Österlunde, Nanomaterials for benign indoor environments: Electrochromics for “smart windows”, sensors for air quality, and photo-catalysts for air cleaning, *Sol. Energy Mater. Sol. Cells* **91**, 355 (2007).
- [9] J. G. Kim, B. Son, S. Mukherjee, N. Schuppert, A. Bates, O. Kwon, M. J. Choi, H. Y. Chung, and S. Park, *J. Power Sources* **282**, 299 (2015).
- [10] S. Ohno, A. Banik, G. F. Dewald, M. A. Kraft, T. Krauskopf, N. Minafra, P. Till, M. Weiss, and W. G. Zeier, Materials design of ionic conductors for solid state batteries, *Prog. Energy* **2**, 022001 (2020).
- [11] L. Cao, O. Petravic, P. Zakalek, A. Weber, U. Rücker, J. Schubert, A. Koutsioubas, S. Mattauch, and T. Brükel, Reversible control of physical properties via an oxygen-vacancy-driven topotactic transition in epitaxial La_{0.7}Sr_{0.3}MnO_{3-δ} thin films, *Adv. Mater.* **31**, 1806183 (2019).
- [12] R. Muenstermann, T. Menke, R. Dittmann, and R. Waser, Coexistence of filamentary and homogeneous resistive switching in Fe-doped SrTiO₃ thin-film memristive devices, *Adv. Mater.* **22**, 4819 (2010).
- [13] D.-H. Kwon, K. M. Kim, J. H. Jang, J. M. Jeon, M. H. Lee, G. H. Kim, X.-S. Li, G.-S. Park, B. Lee, S. Han *et al.*, Atomic structure of conducting nanofilaments in TiO₂ resistive switching memory, *Nat. Nanotechnol.* **5**, 148 (2010).
- [14] Y. Yang, P. Gao, L. Li, X. Pan, S. Tappertzhofen, S. Choi, R. Waser, I. Valov, and W. D. Lu, Electrochemical dynamics of nanoscale metallic inclusions in dielectrics, *Nat. Commun.* **5**, 4232 (2014).
- [15] F. Baiutti, F. Chiabrera, D. Diercks, A. Cavallaro, L. Yedra, L. López-Conesa, S. Estradé, F. Peiró, A. Morata, A. Aguadero *et al.*, Direct measurement of oxygen mass transport at the nanoscale, *Adv. Mater.* **33**, 2105622 (2021).
- [16] R. A. De Souza, J. Zehnpfenning, M. Martin, and J. Maier, Determining oxygen isotope profiles in oxides with time-of-flight SIMS, *Solid State Ion.* **176**, 1465 (2005).
- [17] D. Kalaev, E. Yalon, and I. Riess, On the direction of the conductive filament growth in valence change memory devices during electroforming, *Solid State Ion.* **276**, 9 (2015).
- [18] H.-I. Yoo, M.-W. Chang, T.-S. Oh, C.-E. Lee, and K. D. Becker, Electrocoloration and oxygen vacancy mobility of BaTiO₃, *J. Appl. Phys.* **102**, 093701 (2007).
- [19] S. K. Mohapatra and S. Wagner, Electrochromism in nickel-doped strontium titanate, *J. Appl. Phys.* **50**, 5001 (1979).
- [20] R. Waser, T. Baiatu, and K.-H. Härdtl, Dc electrical degradation of perovskite-type titanates: I, ceramics, *J. Am. Ceram. Soc.* **73**, 1645 (1990).
- [21] R. Waser, T. Baiatu, and K.-H. Härdtl, Dc electrical degradation of perovskite-type titanates: II, single crystals, *J. Am. Ceram. Soc.* **73**, 1654 (1990).
- [22] T. Baiatu, R. Waser, and K.-H. Härdtl, Dc electrical degradation of perovskite-type titanates: III, a model of the mechanism, *J. Am. Ceram. Soc.* **73**, 1663 (1990).
- [23] J. S. Lim, H.-H. Nahm, M. Campanini, J. Lee, Y.-J. Kim, H.-S. Park, J. Suh, J. Jung, Y. Yang, T. Y. Koo *et al.*, Critical ionic transport across an oxygen-vacancy ordering transition, *Nat. Commun.* **13**, 5130 (2022).
- [24] J. Suh, J. S. Lim, H.-S. Park, and C.-H. Yang, Complementary study of anisotropic ion conduction in (110)-oriented Ca-doped BiFeO₃ films using electrochromism and impedance spectroscopy, *Appl. Phys. Lett.* **119**, 022902 (2021).
- [25] J. Guyonnet, in *Ferroelectric Domain Walls: Statics, Dynamics, and Functionalities Revealed by Atomic Force Microscopy* (Springer, Cham, 2014), pp. 89–105.
- [26] M. Kotrla and P. Šmilauer, Nonuniversality in models of epitaxial growth, *Phys. Rev. B* **53**, 13777 (1996).
- [27] I. Bischofberger, R. Ramachandran, and S. R. Nagel, Fingering versus stability in the limit of zero interfacial tension, *Nat. Commun.* **5**, 5265 (2014).
- [28] H. S. Rabbani, D. Or, Y. Liu, C.-Y. Lai, N. B. Lu, S. S. Datta, H. A. Stone, and N. Shokri, Suppressing viscous fingering in structured porous media, *Proc. Natl. Acad. Sci. USA* **115**, 4833 (2018).

- [29] J. Maher, Development of viscous fingering patterns, *Phys. Rev. Lett.* **54**, 1498 (1985).
- [30] H. Schmalzried, in *Chemical Kinetics of Solids* (Verlag, Weinheim, 1995), pp. 265–272.
- [31] J. Janek and C. Korte, Electrochemical blackening of yttria-stabilized zirconia–morphological instability of the moving reaction front, *Solid State Ion.* **116**, 181 (1999).
- [32] J. S. Lim, J. H. Lee, H.-S. Park, R. Gao, T. Y. Koo, L. W. Martin, R. Ramesh, and C.-H. Yang, Ultrafast collective oxygen-vacancy flow in Ca-doped BiFeO₃, *NPG Asia Mater.* **10**, 943 (2018).
- [33] C.-H. Yang, J. Seidel, S. Y. Kim, P. B. Rossen, P. Yu, M. Gajek, Y.-H. Chu, L. W. Martin, M. B. Holcomb, Q. He *et al.*, Electric modulation of conduction in multiferroic Ca-doped BiFeO₃ films, *Nat. Mater.* **8**, 485 (2009).
- [34] J. S. Lim, J. H. Lee, A. Ikeda-Ohno, T. Ohkochi, K.-S. Kim, J. Seidel, and C.-H. Yang, Electric-field-induced insulator to Coulomb glass transition via oxygen-vacancy migration in Ca-doped BiFeO₃, *Phys. Rev. B* **94**, 035123 (2016).
- [35] J. Seidel, W. Luo, S. J. Suresha, P.-K. Nguyen, A. S. Lee, S.-Y. Kim, C.-H. Yang, S. J. Pennycook, S. T. Pantelides, J. F. Scott *et al.*, Prominent electrochromism through vacancy-order melting in a complex oxide, *Nat. Commun.* **3**, 799 (2012).
- [36] M. Campanini, R. Erni, C.-H. Yang, R. Ramesh, and M. D. Rossell, Periodic giant polarization gradients in doped BiFeO₃ thin films, *Nano Lett.* **18**, 717 (2018).
- [37] J. D. Sayre, K. T. Delaney, and N. A. Spaldin, Interplay between strain and oxygen vacancies in lanthanum aluminate, [arXiv:1202.1431](https://arxiv.org/abs/1202.1431).
- [38] M. T. Curnan and J. R. Kitchin, Effects of concentration, crystal structure, magnetism, and electronic structure method on first-principles oxygen vacancy formation energy trends in perovskites, *J. Phys. Chem. C* **118**, 28776 (2014).
- [39] See Supplemental Material at <http://link.aps.org/supplemental/10.1103/PhysRevMaterials.7.123401> for the original video corresponding to the electrocoloration experiment depicted in Fig. 1(c) (note that the playback speed of the video was increased by a factor of 5), and also for the analysis with time dependencies of the position and width of the color fronts.
- [40] H.-S. Park, J. S. Lim, J. Suh, and C.-H. Yang, Real-time observation of filamentary conduction pathways in Ca-doped BiFeO₃, *Appl. Phys. Lett.* **115**, 183901 (2019).
- [42] R. L. Chouke, P. Van Meurs, and C. Van der Poel, The stability of a slow, immiscible, v liquid-liquid displacement in a permeable media, *Petrol. Trans. AIME* **216**, 188 (1959).
- [43] J. Blanc and D. L. Staebler, Electrocoloration in SrTiO₃: Vacancy drift and oxidation-reduction of transition metals, *Phys. Rev. B* **4**, 3548 (1971).